Spectroscopic characterization of Er^{3+} in stabilized zirconia single crystals

1991 J. Phys.: Condens. Matter 3 8491

(http://iopscience.iop.org/0953-8984/3/43/015)

J. Phys.: Condens. Matter 3 (1991) 8491–8502. Printed in the UK

Spectroscopic characterization of Er^{3+} in stabilized zirconia single crystals

R I Merino, V M Orera, R Cases and M A Chamarro
Instituto de Ciencia de Materiales de Aragón, Universidad de Zaragoza-CSIC, Facultad de Ciencias, 50009 Zaragoza, Spain

Received 13 May 1991, in final form 8 July 1991

Abstract. Erbium-doped yttria-stabilized zirconia (YSZ) single crystals of $84ZrO_2/16YO_{1.5}$ composition have been studied by electron paramagnetic resonance (EPR), optical absorption and photoemission techniques at temperatures between 10 and 680 K. At 10 K the Stark-structure of the $^4I_{15/2}$ and $^4S_{3/2}$ multiplets has been resolved and it corresponds to a statistical distribution of nearly-cubic octocoordinated (CN8) and trigonal hepta-coordinated (CN7) Er^{3+} ions. The 300 K spectroscopic properties are studied in the frame of the Judd–Ofelt theory. From the calculated radiative transition probabilities and the measured lifetimes we have determined the non-radiative transition rates and luminescence efficiencies, and compared them with previous results using YSZ of a different composition. The influence of the matrix composition on the spectroscopic characteristics of the Er^{3+} ion is discussed.

1. Introduction

Yttria-stabilized zirconia (YSZ) is a high-temperature material used as a solid state electrolyte in many applications such as oxygen sensors, electrochemical oxygen pumps and fuel cells [1]. The recent success in producing large single crystals of good optical quality opens up new perspectives for the crystals' use as an optical material, specifically when reliability under extreme conditions is required. This material is also a suitable matrix for ions with useful optical properties.

The substitution of Zr^{4+} by Y^{3+} to stabilize the cubic phase results in a high concentration of oxygen vacancies, thus different lattice sites with a point symmetry lower than cubic will be available both for the electronic defects and impurity ions. Since their optical properties depend on their environment, large variations are expected in the relatively intense intraconfigurational $d \rightarrow d$ or $f \rightarrow f$ transitions of ions placed in the different lattice sites.

Consequently, the investigation of the spectroscopic properties of YSZ, either pure or doped with ions of the transition series or rare-earths, is of current interest and studies have been made recently in spite of the difficulties of the highly defective structure of these crystals.

In a recent study on the intrinsic defects, we proposed the simultaneous presence of two different electron traps at hexa and heptacoordinated Zr^{3+} ions [2]. Although electrons are preferably trapped at the hexacoordinated Zr^{3+} the defect concentrations agree with the description of the YSZ anion sublattice being a random distribution of

0953-8984/91/438491 + 12 $03.50

oxygen vacancies on oxygen positions, as established by Dexpert-Ghys *et al* [3]. This result is in line with the existence of two types of Bi^{3+} ions (eight- and seven-fold coordinated) reported for YSZ: Bi [4]. However the situation is far from being general. For instance only a site with a trigonally distorted octahedral symmetry was found for the Cr^{3+} ion [5]. An interesting point related with the preceding considerations arises when we realize that the wide solubility range of yttria in zirconia can be used to produce different impurity sites having different spectroscopic properties simply by changing the crystal composition. This was observed several years ago by Arashi [6] in the course of some studies on the oxygen distribution in YSZ crystals with different concentrations of yttria, using the optical absorption bands of the Er^{3+} ion as a probe. Two distinct sites for the impurity ion were clearly resolved, the amount of ions in each site being strongly dependent on the crystal composition. Unfortunately, no other studies were performed in those samples.

The Er^{3+} ion has some optical properties that have been extensively applied in optical devices [7]. The possibility of using YSZ: Er as a laser material was advanced some years ago by Greenberg *et al* [8]. In this paper we present a detailed study of the spectroscopic properties of YSZ: Er single crystals with a zirconium to yttrium atomic ratio of 84/16 by using optical absorption and emission techniques including lifetime measurements. At low temperatures the Stark-structure of the absorption and emission bands can be partially resolved and using time resolved spectroscopy two types of Er^{3+} ions are clearly distinguished. The electron spin resonance (EPR) also indicates the presence of trigonally distorted Er^{3+} ions and the analysis of the Stark structure and EPR data is in favour of the presence of both nearly cubic octocoordinated (CN8) and trigonally distorted heptacoordinated (CN7) Er^{3+} ions. Their $f \rightarrow f$ transition 'oscillator strengths' are estimated and they are larger for defects of lower symmetry.

At 300 K (RT) and over, all the Stark levels of the absorbing or emitting multiplets are thermally populated and consequently the contributions of each particular site cannot be easily separated. We have used the Judd–Ofelt (J–O) theory [9, 10] to obtain radiative transition probabilities between the multiplets. In the frame of this theory most of the ligand effects are described by phenomenological parameters obtained from the absorption spectrum. Thus, the analysis performed at 300 K corresponds to an 'average' defect where the site differences are smeared out. From the comparison between calculated and measured lifetimes, the non-radiative rates have also been derived. Our results differ from those for Er in YSZ with a 50/50 ratio [8], which is discussed in the light of the matrix composition's influence on the spectroscopic properties of Er^{3+} in YSZ. The effect of thermo-chemical treatments on the emission efficiencies and the stability of Er^{3+} is also explored.

2. Experimental procedure

Crystals of $Zr_{0.82}Y_{0.17}Er_{0.006}O_{1.91}$ and $Zr_{0.81}Y_{0.16}Er_{0.02}O_{1.91}$ used in this study were purchased from Ceres Co, USA. The determination of the Er content of the samples was performed by the method described in reference [11] at the Instituto de Cerámica y Vidrio de Madrid. The samples were orientated by the back-reflection Laue method with the x-rays from a Cu anticathode tube operating at 45 keV and 25 mA. Thermochemical reduction at 1100 °C was achieved by the procedure described in [2]. EPR measurements

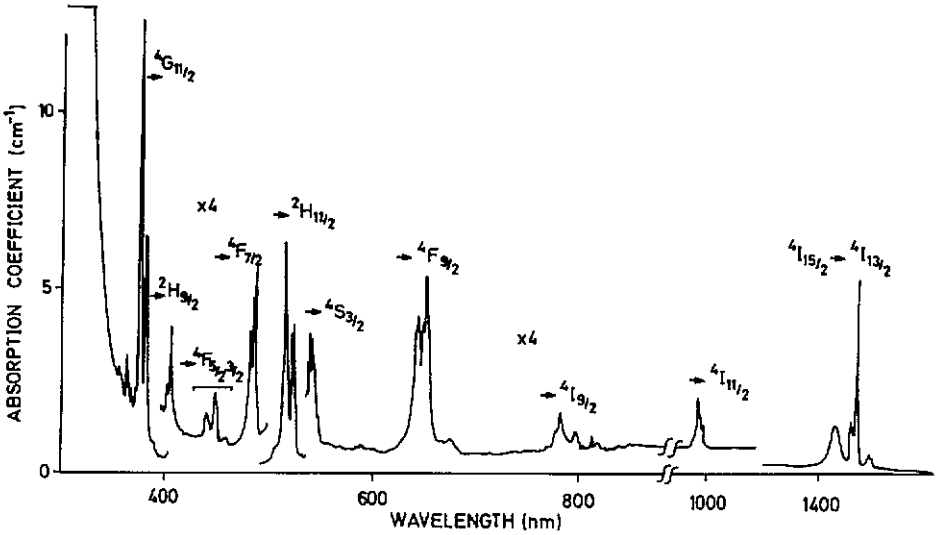

Figure 1. RT absorption spectrum of the sample $Zr_{0.81}Y_{0.16}Er_{0.02}O_{1.91}$.

were performed in a Varian E-112 spectrometer operating in the x-band. Optical absorption measurements were made in a Hitachi U-3400 spectrophotometer. Photoluminescence spectra were obtained by exciting the samples with light either from a 150 W Xe arc-lamp for the visible and near infra-red or from a 500 W tungsten lamp for the far infra-red, passed through a 0.25 m monochromator. Fluorescence was detected through a 0.5 m monochromator with a Hamamatsu R-928 photomultiplier for the visible, or Si or Ge detectors for the infra-red. Lifetimes were measured by modulating the light with a mechanical chopper and using a Tektronic 2430 digital oscilloscope controlled by a computer.

Time resolved spectroscopy and lifetime measurements were also performed by exciting with a tunable dye laser. The pulse duration was 1 ns and the linewidth about 0.1 nm.

3. Experimental results and interpretation

As-grown crystals were transparent, pink coloured and had the absorption edge near 300 nm. The refractive index was $n = 2.17$ and the density $\rho \approx 5.9$ g cm^{-3}. In figure 1 we give the optical absorption spectra of the 2.2 at.mol% YSZ:Er sample measured at RT. The spectrum is typical of Er^{3+} and the transitions associated with the bands are also given in the figure.

3.1. Low temperature measurements. Site identification

Although some structure is observed in the absorption bands of Er^{3+} at RT, the thermal population of the Stark levels makes a detailed analysis of those components difficult. At temperatures near liquid helium temperature (LHeT) only the lowest lying levels of each multiplet will be populated and the structure of the absorption bands will map out

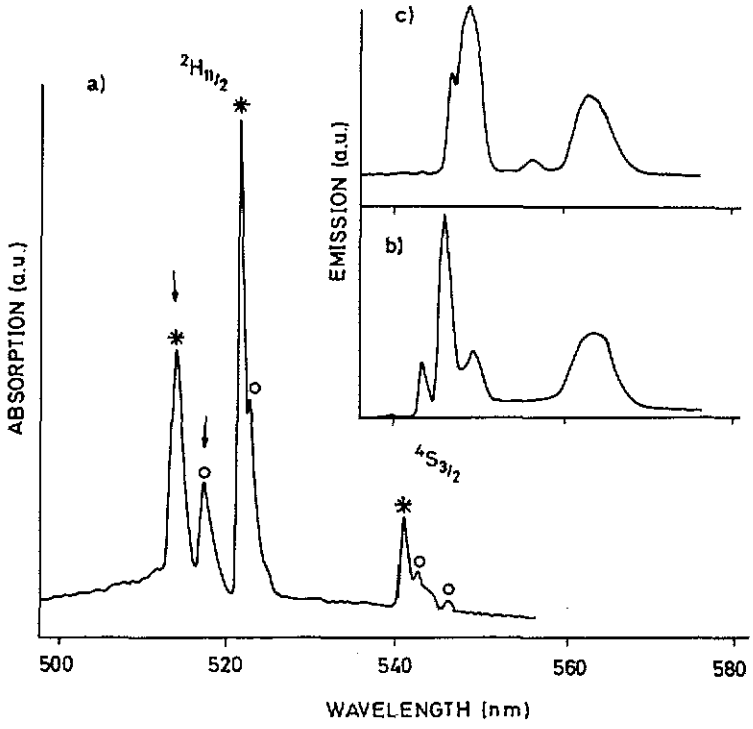

Figure 2. (*a*) $^4I_{15/2} \rightarrow {}^4S_{3/2}$, $^2H_{11/2}$ absorption bands of YSZ:Er at 10 K. * peaks are assigned to CN8 centres and ○ to CN7. Time resolved emissions from the $^4S_{3/2}$ level for the two kinds of sites; (*b*) nearly octocoordinated (CN8), with $\lambda_{exc} = 514$ nm and time gate 280–380 μs; (*c*) nearly heptacoordinated (CN7), with $\lambda_{exc} = 517$ nm and time gate 70–110 μs. The arrows in (*a*) indicate the excitation wavelengths for (*b*) and (*c*).

the Stark components of the excited levels whereas the emission bands will reflect those of the ground multiplet.

In figure 2 we show the absorption and emission spectra at 10 K involving the $^4S_{3/2}$ and $^2H_{11/2}$ excited levels. The absorption spectrum consists of at least three bands at 541, 542.6 and 545.8 nm corresponding to the $^4I_{15/2} \rightarrow {}^4S_{3/2}$ transition, and four bands at 514, 517, 522 and 523 nm corresponding to the $^4I_{15/2} \rightarrow {}^2H_{11/2}$ transition. Important information is given by the structure of the former transition since the $^4S_{3/2}$ level should not split in a cubic crystal field. Thus, the presence of at least three bands indicates the existence of at least two different sites for Er^{3+}. This is further confirmed by the emission measurements. In fact, a different emission spectrum is observed when we excite in the 541 nm band than when we excite either in 542.6 or in 545.8 nm. Besides, the lifetimes of both emissions are also different, being 70 ± 10 μs for the latter and 130 ± 5 μs for the former. The same emission spectra are obtained when we excite in the $^4I_{15/2} \rightarrow {}^2H_{11/2}$ absorption bands where they can be resolved using both the excitation in the different absorption bands and the time-resolved facility as shown in figure 2.

We were not able to resolve the contributions of the different Er^{3+} sites to the transitions involving the remaining multiplets. As an example, we give in figure 3 the absorption and emission bands corresponding to the $^4I_{13/2} \rightarrow {}^4I_{15/2}$ transitions. At 10 K the absorption spectrum consists of two band groups, a broad one centred at 1442 nm

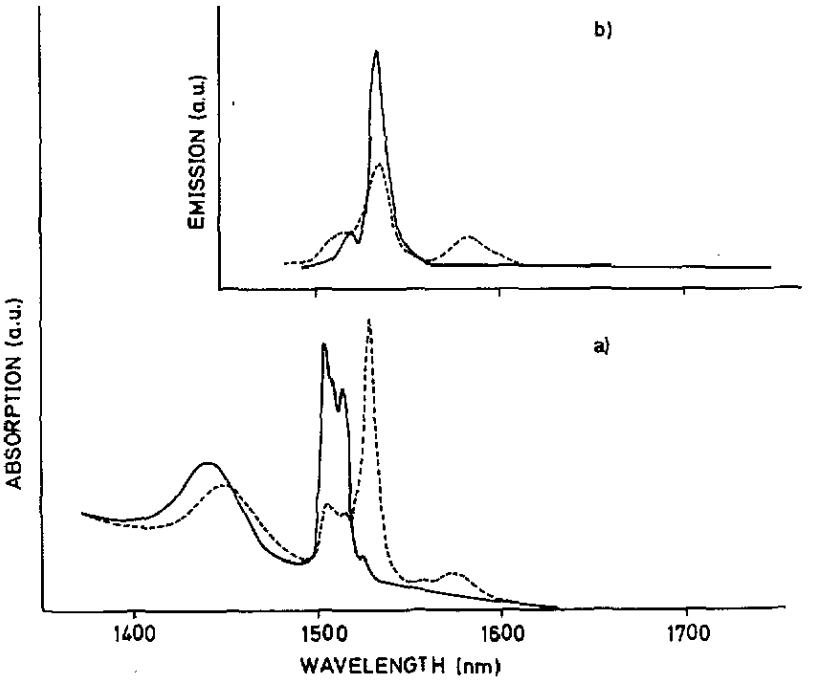

Figure 3. (*a*) $^4I_{15/2} \rightarrow {}^4I_{13/2}$ absorption bands; (*b*) $^4I_{13/2} \rightarrow {}^4I_{15/2}$ emission bands. Measured at 10 K, full curve; RT, broken curve.

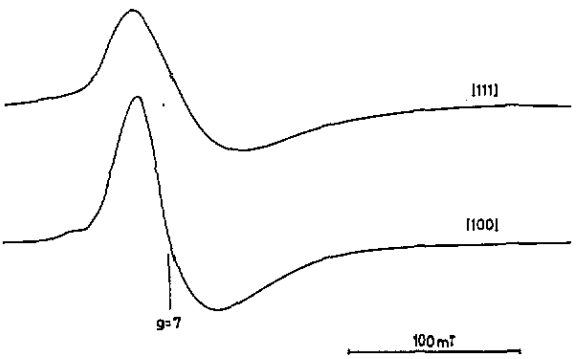

Figure 4. EPR signal of Er^{3+} in YSZ at 20 K for two orientations of the magnetic field.

and an intense triplet at ≈1506 nm. The emission spectrum presents a band at ≈1529 nm with a shoulder at ≈1510 nm. Increasing the temperature produces a decrease in the intensity of these absorption and emission bands at the same time that a narrow absorption band at 1529 nm and a broad absorption and emission at ≈1580 nm emerge.

The EPR spectra consist of broad asymmetric lines centred at $g \approx 7$ but their halfwidths change with magnetic field orientation, being minima for $\mathbf{H} \| [100]$ and maxima when $\mathbf{H} \| [111]$ as shown in figure 4. This behaviour can be explained if there is a trigonal unresolved signal, overlapping an isotropic one centred at $g \approx 7$.

From these results we conclude the following:

(i) There are two sites for Er^{3+} in our YSZ crystals. In fact, the ground-state Stark structures we have described above can be grouped into two sets. One set consists of three narrow levels at 0, 95 and 205 cm^{-1} with a broad level near 660 cm^{-1} for the Er^{3+} ion absorbing in the 541 nm band, and the other set consists of levels at 0, 70, 310 and 525 cm^{-1}.

(ii) The defect whose $^4S_{3/2}$ level is not split by the crystal field (that absorbing at 541 nm) has a cubic symmetry with a Γ_7 doublet as ground state. In fact, in a crystal field of cubic symmetry, the $J = 3/2$ multiplet does not split and the $J = 15/2$ ground state level is split into three quartets Γ_8 and two doublets Γ_6 and Γ_7, and in this symmetry the lowest Stark level can be either Γ_6 or Γ_7 depending on the B_4/B_6 quotient, B_4 and B_6 being the crystal field potential terms [12]. The EPR signal at $g \approx 7$ corresponds to a Γ_7 doublet as the lowest Stark level in agreement with the case of cubic Er^{3+} in other fluorite type matrices [13, 14].

(iii) The Stark structure of the ground state of the defect with a split $^4S_{3/2}$ level is similar to that of tetragonal Er^{3+} in CaF_2 [15]. Since the dependence of the EPR signal on the magnetic field orientation indicates that there is a trigonal defect we conclude that there are also trigonal Er^{3+} ions in our samples.

In the frame of these models the results corresponding to the $^4I_{13/2} \rightarrow {}^4I_{15/2}$ transition are explained as follows. The excited $^4I_{13/2}$ multiplet consists of a triplet with levels at 6644, 6630 and 6607 cm^{-1} and a broad level at 6933 cm^{-1}. Increasing the temperature results in other ground state Stark levels being thermally populated. This results in a very intense absorption band at 1529 nm which is due to transitions between levels placed at $\approx$80 cm^{-1} (an average between the second Stark levels of the ground multiplet at 95 cm^{-1} and 70 cm^{-1} of the two sites) and the second Stark level of the excited state. The same transition also produces the intense emission band. The broad absorption and emission bands at $\approx$1580 nm appearing at RT are due to the transition between the highest energy Stark groups of the excited and ground states. The observed splitting is, again, an average of those of each ion.

Although the contributions of the two sites to either the absorption or the emission bands cannot be resolved, the $^4I_{13/2}$ lifetime measurements clearly support their existence. In fact, exciting at 10 K in the 514 nm band we obtain a lifetime of 10 $\pm$ 0.5 ms whereas exciting in 517 nm we get 6.8 $\pm$ 0.5 ms.

A more complete analysis of the Stark structure involving the crystal field parameters determination, which is out of the scope of the present paper, is on the way.

3.2. RT intensity parameters

At temperatures above 50 K all the Stark levels within each multiplet start to be populated and the absorption spectra correspond to a weighted mixture of the ground state levels of both sites. At RT the thermal population of the Stark levels is more or less completed, and the radiative transition probabilities can be studied using the J–O theory [9, 10] as follows.

The 'oscillator strengths' of the J–J' transitions given in table 1 were obtained from the RT absorption bands using the expression

$$f(J,J') = \frac{mc^2}{\pi e^2 N} \int \frac{\mathrm{OD}(\lambda)2.303}{L\lambda^2}\,\mathrm{d}\lambda \qquad (1)$$

where m and e are the electron mass and charge respectively, c is the light velocity,

Table 1. Absorption band positions, experimental and calculated oscillator strengths of Er^{3+} in YSZ (84/16)single crystals.

λ(nm)	$^4I_{15/2}\rightarrow$	$f_{exp} \times 10^8$	$f_{cal} \times 10^8$
377	$^4G_{7/2}\ ^2G_{9/2}$ $^2K_{15/2}\ ^4G_{11/2}$	798 + 8^{md}	777.5 + 8^{md}
408	$^2H_{9/2}$	31.2	22.5
450	$^4F_{3/2}\ ^4F_{5/2}$	29.7	26.3
487	$^4F_{7/2}$	54.1	67.0
517	$^2H_{11/2}$	355.0	391.7
543	$^4S_{3/2}$	23.2	13.9
651	$^4F_{9/2}$	80.2	89.2
783	$^4I_{9/2}$	11.5	15.7
960	$^4I_{11/2}$	17.3	20.7
1529	$^4I_{13/2}$	36.7 + 66.8^{md}	40.8 + 66.8^{md}

^{md} magnetic dipole contribution.

Table 2. Judd–Ofelt intensity parameters of Er^{3+} in several hosts.

Host	Ω_2 ($\times 10^{-20}$ cm^2)	Ω_4 ($\times 10^{-20}$ cm^2)	Ω_6 ($\times 10^{-20}$ cm^2)
84/16 YSZ	1.50	0.50	0.22
50/50 YSZ [8]	2.92	0.78	0.57
ZBLA [18]	2.54	1.39	0.97

OD(λ) the optical density as a function of wavelength λ, and L the thickness of sample. N is the number of absorbing ions in the unit volume.

On the other hand the 'oscillator strength' $f(aJ, bJ')$ of the a–b transition (at a mean frequency ν) is given by

$$f(aJ, bJ') = [8\pi^2 m\nu/3h(2J+1)e^2n^2][X_{ed}S_{ed} + X_{md}S_{md}] \tag{2}$$

where n is the refractive index of the host at the mean frequency of the transition, $X_{ed} = n(n^2+2)^2/9$ and $X_{md} = n^3$. The magnetic dipole transitions only contribute here to the $^4I_{15/2}\rightarrow {}^4I_{13/2}$ absorption band. The values of S_{md} are usually small and not sensitive to the host: we have used those values given in reference [16].

In the frame of the J–O theory the electric dipole line strength S_{ed} is given by

$$S_{ed}(J, J') = e^2 \sum_{t=2,4,6} \Omega_t \, |\langle (SL)J \| U^{(t)} \| (S'L')J' \rangle|^2 \tag{3}$$

where Ω_2, Ω_4, Ω_6 are three parameters (J–O parameters) to be obtained from a comparison with the experimental results. It is known that the reduced matrix elements of the unit tensors $U^{(t)}$ ($t = 2, 4, 6$) are almost insensitive to the ion environment. The values given in [17] have been used in the calculations. The J–O parameters found by least-square fitting the calculated f values given by (2) to the experimental ones, are compared in table 2 with those obtained for YSZ of a different composition and for ZBLA glasses [18]. The oscillator strengths calculated using those values are also given in table

Table 3. Calculated and measured lifetimes at RT and quantum efficiencies (η) of several levels of Er^{3+} in YSZ crystals of two different compositions.

Level	τ_{rad}	τ_{exp}	η(84/16)	η(50/50) [19]
$^2H_{9/2}$	500 μs			
$^2H_{11/2}$, $^4S_{3/2}$	840 μs	65 ± 10 μs	0.083	0.44
$^4F_{9/2}$	875 μs	6 ± 1 μs	0.007	0.27
$^4I_{11/2}$	11.5 ms	800 ± 50 μs	0.07	
$^4I_{13/2}$	6.8 ms	9 ± 0.5 ms		

1 and the root mean square value of the fitting is 1.8×10^{-7} which is within the usual range for that type of analysis.

It can be seen that our J–O parameters and hence the oscillator strengths are about a factor of two smaller than those of zirconia of a 50/50 cation ratio. As we will see later, this effect can be related to the higher concentration of low symmetry sites in the 50/50 YSZ compounds. The oscillator strengths are, on the other hand, almost temperature independent. In fact, determinations at temperatures up to 630 K give essentially the values as at RT.

3.3. Emission probabilities and experimental lifetimes

We have measured the emission spectra in the 300–2000 nm region and the multiplet lifetimes at temperatures above LHeT. Thermal population of the Stark levels in both the ground and excited multiplets results in emission bands where the contribution of each ion site cannot be separated and some of the emission decays cannot be exactly fitted by an exponential law with a single relaxation time. As in the case of absorption at RT and over, the emission bands correspond to a mixture of the two sites.

The Ω_t values can now be used to calculate the spontaneous emission probabilities $A(aJ, bJ')$ of the different electronic transitions, which are given by the expression

$$A(aJ, bJ') = [64\pi^4\nu^3/3(2J+1)hc^3][X_{ed}S_{ed} + X_{md}S_{md}] \tag{4}$$

and are related to the radiative lifetime τ_R of the excited state a by

$$\frac{1}{\tau_R} = \sum_b A(a, b) \tag{5}$$

where the summation is over the electric and magnetic dipole transitions to all terminal states b. Although the 'oscillator strengths' and the calculated radiative lifetimes are temperature independent the experimental lifetimes, except for the $^4I_{13/2}$ multiplet, shorten with temperature. The RT measured and calculated lifetimes are given in table 3 together with the emission quantum efficiencies of the levels defined by $\eta = \tau_{exp}/\tau_R$ that are also compared with those of the 50/50 YSZ [19].

The emission bands and the lifetimes are the same within the error limits for the two Er concentrations studied indicating that transfer relaxation is negligible here.

3.4. Multiphonon relaxations

As we have seen, the emission quantum efficiencies are extremely low except for the $^4I_{13/2}$ level. This is due to the existence of non-radiative transitions caused by multi-

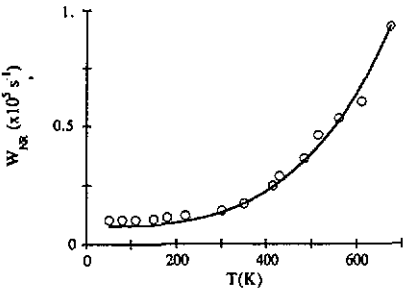

Figure 5. Non-radiative emission probabilities for the $^4S_{3/2}$ level against temperature and its fitting to (7) with $W_{NR}(0) = 7.7 \times 10^{-3}\ s^{-1}$, $p = 6$ and $\hbar\omega = 520\ cm^{-1}$.

phonon decay processes. The multiphonon relaxation rate W_{NR} (NR means non-radiative) from a given level a to its next lower level may be obtained, in the absence of energy transfer, using the relation

$$W_{NR} = 1/\tau_{exp} - 1/\tau_R \tag{6}$$

where τ_{exp} is the experimental lifetime of the level a.

On the other hand, the temperature dependence of the multiphonon relaxation between the electronic levels of RE in crystals may be adequately described by the single frequency model developed by Riseberg and Moos [20], through the expression

$$W_{NR}(T) = W_{NR}(0)\{\exp(\hbar\omega/kT)/[\exp(\hbar\omega)/kT) - 1]\}^p \tag{7}$$

where $\hbar\omega$ is the energy of the active phonons in the transition, $p = \Delta E/\hbar\omega$ is the number of phonons which must be emitted in order to span the energy gap (ΔE) between adjacent levels and $W_{NR}(0)$ is the low-temperature multiphonon emission rate.

In figure 5 we plot the non-radiative relaxation rates of the $^4S_{3/2}$ level obtained from (6) and the experimental and radiative lifetimes as a function of temperature. The radiative lifetime of the $^4S_{3/2}$ level has been corrected for the effect of the thermalization with the $^2H_{11/2}$ upper level and as the experimental lifetime we have taken the result of fitting the decay covering three e-folds to an exponential law.

The non-radiative decay rates can be fitted to (7) using the parameters $p = 6$ and $\hbar\omega = 520\ cm^{-1}$ and $W_{NR}(0) = 7.7 \times 10^{-3}\ s^{-1}$. Similar behaviour is obtained for the other transitions, being the average phonon energy close to that of the stretching vibrations of the oxygen cubes ($\approx 600\ cm^{-1}$) as measured by the Raman technique [21]. Finally, we have performed thermal annealing of the samples in a reducing atmosphere up to 1370 K. Besides the formation of the Zr^{3+} absorption band [2] no other changes related to the optical properties of the Er^{3+} ion were detected.

4. Discussion

The simultaneous presence of two different sites for Er^{3+} ions in our YSZ crystals has been clearly established by the optical absorption and emission experiments. It can be easily understood if we assume that, as suggested by the Arashi experiments [6], the Er^{3+} ions like Bi^{3+} [4] are randomly distributed over the cation sites which, themselves, are also randomly perturbed by oxygen vacancies. Based only on statistical grounds the probability of having none, one or two oxygen vacancies close to a cation site is found

to be, for the 84/16 YSZ, equal to 0.69, 0.26 and 0.04 respectively [2]. Thus, we can expect about 2.6 times more cubal than trigonal Er^{3+} ions.

Although the spectroscopic results can be interpreted by the presence of both cubal and trigonal Er^{3+} ions, owing to the high concentration of oxygen vacancies, the ions will not be in a real cubal symmetry. Rather, we should talk about octocoordinated (CN8) and heptacoordinated (CN7) sites and allow for the unresolved low symmetry distortions caused by the defects present in sites other than the first coordinated shell. These low symmetry perturbations produce the unusually large band halfwidths and the relatively high 'oscillator strengths' observed in the CN8 defect.

The RT characterization we have carried out in sections 3.2, 3.3 and 3.4 provides us with a set of parameters which ideally describe a kind of 'average defect'. In order to study in more detail which are the optical properties of Er^{3+} in each particular site we have to proceed as follows.

First, let us assume that the distribution of Er impurities is random. Thus, we know the concentration of CN8 and CN7 defects. Since the absorption band at 541 nm in figure 2 corresponds to the CN8 defect, applying (1) we obtain an 'oscillator strength' $f(8) \approx 17 \times 10^{-8}$ for this transition. The band is due to the transition between the ground state lowest level Γ_7 and the unsplit $^4S_{3/2}$ multiplet. Taking into account the degeneracies of the levels involved we obtain a radiative transition probability for that level of $\approx 90\ s^{-1}$.

The excitation of the $^4S_{3/2}$ level decays radiatively into the different multiplets below it. From the calculations performed in section 3.3 we know that the 'branching ratio' of the emission from the $^4S_{3/2}$ level to the ground multiplet is about 0.7 but, as can be seen in figure 2, only about 6% of that goes to the Γ_7 bottom level. The total radiative emission probability of the $^4S_{3/2}$ level is then $A(8) \approx 2.1 \times 10^3\ s^{-1}$. From the measured lifetime and (6) we can straightforwardly obtain the non-radiative transition probability at low temperature, $W_{NR}(0) \approx 5.6 \times 10^3\ s^{-1}$ for that level.

If we apply the same procedure to the remaining absorption bands, which we assume are due entirely to the CN7 defect, we obtain an 'oscillator strength' $f(7) \approx 40 \times 10^{-8}$ that is ≈ 2.3 times that of the CN8 defect. However, we cannot resolve from the emission spectrum the band corresponding to the transition to the lowest ground-state Stark level and obtain as before, the radiative emission probability.

We have used another procedure based on the measurement of the emission band areas for each defect. Taking into account the light power absorbed and that the degeneracy of the emitting $^4S_{3/2}$ level is two for CN7 and four for CN8, it results that the ratio between their radiative emission probabilities must be $A(7)/A(8) = 4.3$. Since the excitation and the emission bands occur in the same spectral region for the two sites no other corrections for the experimental set-up response are needed. It is also interesting to point out that in the present calculation we do not have any previous assumptions on the ion distribution. This value corresponds to an 'oscillator strength' ratio $f(7)/f(8) = 2.15$, which is very close to that obtained from the absorption spectrum but assumes a random distribution of defects. The similarity between the 'oscillator strength' ratios obtained by the different procedures gives support to a defect model consisting of a random distribution of Er^{3+} ions among the cation sites.

Coming back to the calculations, we obtain $A(7) \approx 9 \times 10^3\ s^{-1}$ for the radiative transition probability at LHeT and $W_{NR}(0) \approx 5.3 \times 10^3\ s^{-1}$ for the non-radiative one. Due to the experimental errors involved in the calculation of the areas, lifetimes etc, the values we have obtained so far have to be taken with some precaution, but the following conclusions are out of the error limits. As expected the 'oscillator strength' is larger for the axial CN7 ion than for the more symmetric CN8 defect. With respect to the non-radiative transition probabilities, the overlapping of the bands of the two defects at

temperatures higher than 50 K prevents us from performing a Riseberg and Moos-type of analysis to obtain the average phonon which interacts with each site. However, the values we have calculated for the low temperature non-radiative probabilities tell us that these probabilities do not depend very much on the defect symmetry, a situation frequently, though not generally, found in solids. On the other hand, they are very close to the value obtained from the extrapolation to low temperature of the high temperature non-radiative decay data given in figure 5.

Next, we will discuss the RT results. From a practical point of view and for most applications in optical devices it is desirable to have large transition probabilities. In 84/16 YSZ crystals there are two sites with quite different optical properties but at RT their absorption and emission bands overlap. In order to get an enhancement of the radiative transition probabilities we should prepare YSZ crystals with a composition enabling for a majority of CN7 sites. This would happen in a crystal with a 60/40 composition but we cannot say now what will be the effect of the rest of the oxygen vacancies placed out of the first coordination shell. However, the influence of the matrix composition may not be restrictive to the radiative processes only. In fact, the non-radiative transition probabilities also depend on the matrix composition through the electron–phonon interaction. That the lattice phonons strongly depend on the yttria content was illustrated in reference 21 where the Raman spectra of YSZ crystals with different compositions was measured. It was found that the density of the high energy modes decreases as the yttria content increases. Thus, we would expect a lower average phonon energy and, accordingly, lower non-radiative rates and higher quantum efficiencies for emissions in the visible part of the spectrum in crystals that have higher yttria content. This could well explain the differences in quantum efficiencies of the different samples reported in table 3.

As a conclusion, we predict large variations both in the intensity parameters and multiphonon relaxation rates of Er doped YSZ crystals with the matrix composition. Within some limits the optical properties of the 4f impurities in the zirconia matrices could be tailored by changing the yttria proportion.

Acknowledgments

This work was sponsored by the Dirección General de Investigación Científica y Técnica under contract No. PB0361 with the CSIC. We wish to thank Pilar Ortega from the Instituto de Cerámica y Vidrio de Madrid for the chemical analysis of the samples used in this work.

References

[1] Claussen N, Rühle M and Heuer A H (ed) 1984 vol 12 Science and technology of zirconia II *Advances in Ceramics* (Columbus OH: The American Ceramic Society)
[2] Orera V M, Merino R I, Chen Y, Cases R and Alonso P J 1990 *Phys. Rev.* B **42** 9782
[3] Dexpert-Ghys J, Faucher M and Caro P 1984 *J. Solid State Chem.* **54** 179
[4] Blasse G, Hao Zhiran, Winnubst A J A and Burggraaf A J 1984 *Mat. Res. Bull.* **19** 1057
[5] Alonso P J, Alcalá R, Casas-Gonzalez J, Cases R and Orera V M 1989 *J. Phys. Chem. Solids* **50** 1185
[6] Arashi H 1972 *Phys. Status Solidi* a **10** 107
[7] Kaminskii A A 1981 *Laser Crystals (Springer Series in Optical Sciences 14)* ed D L MacAdam (Berlin: Springer)

[8] Greenberg E, Katz G, Reisfeld R, Spector N, Marshall R C, Bendow B and Brown R N 1982 *J. Chem. Phys.* **77** 4797
[9] Judd B R 1962 *Phys. Rev.* **127** 750
[10] Ofelt G S 1962 *J. Chem. Phys.* **37** 511
[11] Martinez-Lebrusant C and Barba F 1990 *Analyst* **115** 1335
[12] Lea K R, Leask M J M and Wolf W P 1962 *J. Phys. Chem. Sol.* **23** 1381
[13] Ranon U and Low W 1963 *Phys. Rev.* **132** 1609
[14] Abraham M M, Weeks R A, Clark G W and Finch C B 1966 *Phys. Rev.* **148** 350
[15] Smirnov A I 1970 *Sov. Phys. Solid State* **12** 590
[16] Carnall W T, Fields P R and Rajnak K 1968 *J. Chem. Phys.* **49** 4412
[17] Carnall W T, Croswhite H and Croswhite H M 1978 Argonne National Laboratory Report ANL-78-XX-95
[18] Shinn M D, Sibley W A, Drexhage M G and Brown R N 1983 *Phys. Rev.* B **27** 6635
[19] Reisfeld R, Katz K, Jacoboni C, de Pape R, Dexhage M G, Brown R N and Jorgensen C K 1983 *J. Solid State Chem.* **48** 323
[20] Riseberg L A and Moos H W 1968 *Phys. Rev.* **174** 429
[21] Aleksandrov V I, Voron'ko Yu K, Ignat'ev B V, Lomonova E E, Osiko V V and Sobol' A A 1978 *Sov. Phys. Solid State* **20** 305